

A More La Niña–Like Response to Radiative Forcing after Flux Adjustment in CESM2[©]

JING-YI ZHUO^{©,a}, CHIA-YING LEE,^a ADAM SOBEL,^{a,b} RICHARD SEAGER,^a SUZANA J. CAMARGO,^a YEN-HENG LIN,^c
BONIFACE FOSU,^c AND KEVIN A. REED^d

^a Lamont-Doherty Earth Observatory, Columbia University, Palisades, New York

^b Department of Applied Physics and Applied Mathematics, Columbia University, New York, New York

^c Department of Geosciences, Mississippi State University, Mississippi State, Mississippi

^d School of Marine and Atmospheric Sciences, Stony Brook University, Stony Brook, New York

(Manuscript received 10 June 2024, in final form 7 November 2024, accepted 10 December 2024)

ABSTRACT: In response to greenhouse gas forcing, most coupled global climate models project the tropical Pacific SST trend toward an “El Niño–like” state, with a reduced zonal SST gradient and a weakened Walker circulation. However, observations over the last five decades reveal a trend toward a more “La Niña–like” state with a strengthening zonal SST gradient. Recent research indicates that the identified trend differences are unlikely to be entirely due to internal variability and probably result, at least in part, from systematic model biases. In this study, Community Earth System Model, version 2 (CESM2), is used to explore how mean-state biases within the model may influence its forced response to radiative forcing in the tropical Pacific. The results show that using flux adjustment to reduce the mean-state bias in CESM2 over the tropical regions results in a more La Niña–like trend pattern in the tropical Pacific, with a strengthening of the tropical Pacific zonal SST gradient and a relatively enhanced Walker circulation, as hypothesized to occur if the ocean thermostat mechanism is stronger than the atmospheric mechanisms which by themselves would weaken the Walker circulation. We also find that the historical strengthening of the tropical Pacific zonal gradient is transient but persists into the near term in a high-emissions future warming scenario. These results suggest the potential of flux adjustment as a method for developing alternative projections that represent a wider range of possible future tropical Pacific warming scenarios, especially for a better understanding of regional patterns of climate risk in the near term.

KEYWORDS: Pacific Ocean; Tropics; Atmosphere-ocean interaction; Climate change; Climate models; Trends

1. Introduction

The mean state of the tropical Pacific is characterized by a zonal gradient in the equatorial sea surface temperature (SST) between the warm pool in the west and the cold tongue driven by oceanic upwelling in the east. This mean state is maintained by coupled ocean-atmosphere interactions that depend on the Bjerknes feedback (Bjerknes 1966), connecting the surface winds of the Walker circulation and the zonal SST gradient. As exemplified by the interannual El Niño–Southern Oscillation (Sarachik and Cane 2010) and variations in global ocean heat uptake on decadal time scales (England et al. 2014; Hu and Fedorov 2017), the tropical Pacific has a significant influence on global weather and climate. Over the past four to five decades, the equatorial Pacific has evolved toward a more La Niña–like state with the strengthening zonal SST gradient, moderating the rate of global warming (Kosaka and Xie 2013), activating North Atlantic tropical cyclone activity while muting that in the North Pacific (Murakami et al. 2020; Sobel et al. 2023), and drying the western United States (Seager et al. 2023). However, state-of-the-art climate models

do not reproduce the observed tropical Pacific surface temperature change; most phase 5 of the Coupled Model Inter-comparison Project (CMIP5) and CMIP6 models tend to show a weakening of the gradient over these periods, and it continues into the future projections with increasing magnitude (Seager et al. 2019, 2022; Wills et al. 2022; Lee et al. 2022).

From a thermodynamic perspective, the west Pacific will warm less than the east Pacific in response to increased greenhouse gases (GHGs) due to more effective evaporative cooling over the background warm water (Knutson and Manabe 1995; Xie et al. 2010). The Walker circulation is also expected to slow down as the climate warms due to the reduction in the rate of radiatively driven subsidence in the tropics (Knutson and Manabe 1995; Betts 1998) and the weakening of the tropical convective mass flux (Vecchi and Soden 2007). In contrast, the “ocean thermostat” (OT) mechanism of Clement et al. (1996) and Cane et al. (1997) suggests that equatorial upwelling should partially offset warming in the cold tongue—but not elsewhere—and the west-to-east SST gradient should strengthen accordingly. Heede et al. (2020, 2021) argue that the ocean thermostat is possibly a transient phenomenon because the subsurface ocean will gradually warm, and the OT-induced zonal SST strengthening trend will cease and reverse to be an El Niño–like trend. Despite the time-dependent argument postulating different trends due to different mechanisms in different periods, it is rarely captured by simulations in current state-of-the-art coupled global climate

[©] Supplemental information related to this paper is available at the Journals Online website: <https://doi.org/10.1175/JCLI-D-24-0331.s1>.

Corresponding author: Jingyi Zhuo, jz3699@columbia.edu

models (e.g., Seager et al. 2022; Wills et al. 2022). Nonetheless, such a transient forced response remains crucial for near-term climate adaptation. Recent studies have also identified Southern Ocean cooling as an effective conduit for cooling the tropical southeastern Pacific (Kang et al. 2023) and modulating the zonal gradient of equatorial Pacific SST and the strength of the Walker circulation (Kang et al. 2020), in which the processes may be interactive since the equatorial Pacific can influence the Southern Ocean by teleconnections (Li et al. 2021; Dong et al. 2022). Anthropogenic sulfate aerosols, mainly emitted from the Northern Hemisphere extratropics and reduced since the 1980s, are also potential drivers of the tropical Pacific SST pattern change through the interhemispheric energy transport (Heede and Fedorov 2021; Hwang et al. 2024). Another plausible explanation for the mismatch between observed and modeled trends is internal multidecadal variability (e.g., Bordbar et al. 2017; Olonscheck et al. 2020; Watanabe et al. 2021). However, recent studies have shown that it is highly unlikely that the internal variability alone can fully account for the discrepancy (Seager et al. 2019, 2022; Wills et al. 2022).

A different argument is pursued in Seager et al. (2019). Using a simplified atmosphere–ocean coupled model that can reproduce the observed trend in response to GHG forcing, Seager et al. (2019) provides evidence that state-of-the-art models produce El Niño-like trends of the equatorial SST as a consequence of the common biases in their representations of the background tropical Pacific climate, namely, the excessive cold tongue and double-ITCZ biases (Li and Xie 2014). They argue that a too-cold cold tongue with warmer water and convergence zones north and south creates, by moisture advection and/or diffusion and wind divergence, a local cold tongue environment of too-high relative humidity and too-low wind speed and that this leads to erroneous trends in the right sense to explain the mismatch between observations and simulations of the recent historical period. However, this hypothesis has not yet been validated using a complex coupled climate model.

In this study, we examine how the systematic mean-state biases may modify the radiatively forced tropical Pacific SST pattern using Community Earth System Model, version 2 (CESM2). This is done with paired ensemble simulations: one ensemble retains the common SST background bias, while the other has the bias largely reduced by flux adjustment; both are subjected to identical historical and future forcings. We show that removing the mean-state biases in CESM2 results in a trend toward a more La Niña-like response in the tropical Pacific, which is projected to continue into the near-term future. This provides additional evidence supporting the hypothesis that the false excessive eastern Pacific warming in state-of-the-art models may be associated with the systematic cold tongue and double-ITCZ biases (Seager et al. 2019).

The remainder of the article is structured as follows. Section 2 describes the experimental design, datasets, and methods. Section 3 examines the mean-state bias in the standard CESM2 and its “flux-adjusted” version. In section 4, we compare the historical forced responses in the two experiments both for the ocean and atmosphere. We discuss the

possible contributions from the background bias in section 5. Section 6 provides the near-future projections (mid-twenty-first century) of the tropical Pacific zonal SST gradient. We conclude by summarizing our findings and discussing future work in section 7.

2. Methods

a. Observational data

We use five SST products: 1) Hadley Centre Sea Ice and SST dataset, version 1 (HadISSTv1), data (Rayner et al. 2003), 2) the National Oceanic and Atmospheric Administration Extended Reconstructed SST, version 5 (ERSSTv5) (Huang et al. 2015), 3) the Japanese Meteorological Agency Centennial In Situ Observation-Based Estimates (COBE) data (Ishii et al. 2005) and 4) COBE2 data (Hirahara et al. 2014), and 5) the European Centre for Medium-Range Weather Forecasts (ECMWF) Ocean Reanalysis System 5 (ORAS5) dataset, following Seager et al. (2022). Among these SST datasets, HadISST uses both in situ and satellite data, while COBE uses only in situ data, COBE2 and ERSSTv5 use only satellite data, and ORAS5 assimilates subsurface ocean data and corrects SST based on HadISST. For wind stress products, we use the fifth major global reanalysis produced by ECMWF (ERA5) data (Hersbach et al. 2020). For precipitation, we use the Global Precipitation Climatology Project (GPCP) combined precipitation dataset (Schneider et al. 2013). All these products have a monthly resolution, and we consider a 50-yr period (1970–2019) to compute the climatology or trends from these observational datasets, except for the precipitation climatology for which we use 1979–2019 due to the start date of the GPCP dataset. All the observed atmospheric variables are bilinearly interpolated to the resolution of the CESM2 atmosphere component ($\sim 2^\circ$), while oceanic variables are interpolated to the CESM2 oceanic component resolution ($\sim 1^\circ$). As to be described in section 2c, we use HadISST SST and ERA5 wind stress to calculate the heat and momentum flux adjustments for CESM2 following Vecchi et al. (2014).

b. CMIP6 model data

Following Seager et al. (2022), we examine the modeled SST trend in the 223 simulations of 45 climate models from CMIP6 using the historical simulations extended with the shared socioeconomic pathway 8.5 (SSP8.5) (Eyring et al. 2016). The differences between the future scenarios of SSP2-4.5, SSP3-7.0, and SSP5-8.5 are small through the year 2020 (Wills et al. 2022). A table listing all CMIP6 SST data used in this study is provided in the online supplemental material.

c. Model description and the experimental designs

The CESM2 (Danabasoglu et al. 2020) used in this study consists of the Community Atmosphere Model, version 6 (CAM6), with interactive the Community Land Model, version 5 (CLM5), and the Parallel Ocean Program, version 2 (POP2; gx1v7), with Marine Biogeochemistry Library (MARBL), interactive sea ice [Community Ice Code,

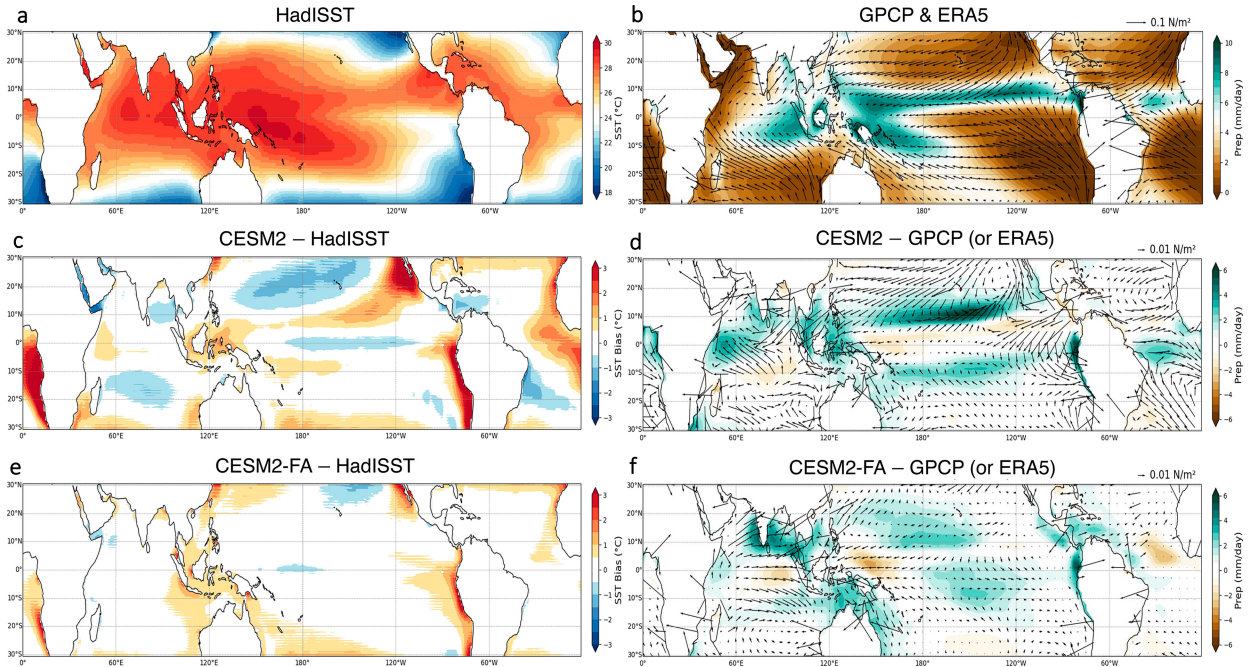


FIG. 1. Reference data: (a) annual-mean HadISST SST ($^{\circ}$ C) over 1970–2019, (b) GPCP precipitation (mm day^{-1}) and ERA5 wind stress (vectors; N m^{-2}) over 1979–2019. Annual-mean model bias: (c) CESM2 SST bias ($^{\circ}$ C), (d) CESM2 precipitation (mm day^{-1}) and wind stress bias (N m^{-2}), (e) CESM2-FA SST bias ($^{\circ}$ C), and (f) CESM2-FA precipitation (mm day^{-1}) and wind stress bias (N m^{-2}) in comparison to the reference data.

version 5.1 (CICE5.1)], and nonevolving land ice [Community Ice Sheet Model (CISM2.1)]. For the atmosphere model, the horizontal resolution is 1.9° latitude $\times 2.5^{\circ}$ longitude. For the ocean model, the horizontal resolution is nominally 1° but increases to $\sim 0.3^{\circ}$ at the equator (i.e., f19_g17).

The 2° CESM2 model used here, just as other many models in CMIP5 and CMIP6, has persistent SST and precipitation biases in the tropical Pacific mean state (e.g., Zhang et al. 2023), such as an excessive cold tongue bias and double ITCZ (Figs. 1c,d). The SST and precipitation biases of the 2° CESM2 are also very similar to those of the standard 1° CESM2 model (Danabasoglu et al. 2020), which have been used for the CESM2 large ensemble (Rodgers et al. 2021). Hereafter, we refer to the 2° CESM2 model without flux adjustments as CESM2.

To isolate the influence of the systematic mean-state model bias on the forced response of the climate model, we develop an alternative configuration of the CESM2, which has resolution, numerics, and parameter settings identical to the CESM2, except that it is flux adjusted. That is, climatological adjustments are made to the CESM2's heat and momentum fluxes from atmosphere to ocean to bring the model's long-term climatology of SST and surface wind stress closer to observational estimates while still allowing the model to vary at higher frequencies (Spencer et al. 2007; Vecchi et al. 2014). The method has also been widely applied in seasonal forecasting (e.g., Magnusson et al. 2013; Vecchi et al. 2014) and climate modeling in earlier decades (e.g., Knutson and Manabe 1995). In the following, we refer to this alternative flux-adjusted CESM2 configuration as CESM2-FA.

We apply a three-step procedure to build CESM2-FA, following Vecchi et al. (2014):

- 1) A simulation with CESM2 is first performed to restore the model's SST to the 1950–2014 monthly estimates from HadISST using Newtonian relaxation with a 5-day restoring time scale. The output from this step is then compared to ERA5 over 1965–2014 to derive the monthly climatological differences in the zonal and meridional momentum flux between the atmosphere and ocean. These climatological differences are referred to as TAU_Adjust (see the appendix; Figs. A1c,d).
- 2) Then, the nudging experiment is repeated to estimate the climatological heat flux needed when TAU_Adjust is applied. In this step, the climatological TAU_Adjust is added to the CESM2 simulation while SST is restored to the observational estimates by repeating the same Newtonian relaxation approach in step 1. This simulation is then used to calculate the heat correction terms by applying climatological average of the SST restoring terms over 1965–2014, which is referred to as SST_Adjust (see the appendix; Figs. A1a,b).
- 3) The final flux-adjusted experiment is performed by adding the monthly climatological TAU_Adjust and SST_Adjust to CESM2. This produces the final simulation referred to as CESM2-FA.

Note that the heat and momentum flux adjustments, as well as the Newtonian relaxation used in steps 1 and 2 are imposed over the whole tropics, within 25° of the equator, linearly interpolating to zero at 30° from the equator. The climatological heat

and momentum flux adjustments are calculated over 1965–2014, with the first 15 years of simulations discarded to allow the model adequate time to adjust to the added flux terms. The climatological flux adjustments show little change whether averaging over the periods 1960–2014, 1965–2014, or 1970–2014 (not shown). The globally averaged top-of-atmosphere radiative imbalance and ocean heat content in the top 300 m show relatively small differences between CESM2 and CESM2-FA, suggesting that flux adjustments do not introduce climate drift. Furthermore, we found that flux adjustments effectively reduce mean-state biases in the preindustrial control (pi-control) setting (not shown), providing evidence that the flux adjustment method is robust regardless of the forcing level. As shown in Figs. 1e and 1f, CESM2-FA has much smaller mean SST and wind stress biases than the standard CESM2. The magnitude of the double ITCZ bias in precipitation is also greatly reduced.

d. 15-member ensemble simulations

To separate the forced response from internal variability, we create 15-member ensemble simulations for CESM2 and CESM2-FA applying the method described in Rodgers et al. (2021). Specifically, we use three initial conditions with the same model configuration from the publicly available 1950 restart files provided by NCAR (see data availability). These initial states have been fully spun up in the CESM2 2° baseline historical simulations (Danabasoglu et al. 2020). We then generate five ensemble members for each of the three initial states by introducing a temperature perturbation of magnitude of 10^{-14} K in the atmospheric model following Kay et al. (2015). Each member's simulations cover the period from 1950 to 2049 and follow the historical and SSP5-8.5 forcing protocols provided by CMIP6 (Eyring et al. 2016). We only use data from the last 80 years (January 1970–December 2049) of simulations to further reduce the possible impact of the memory of the initial state (Kay et al. 2015). Note that despite the flux adjustments described above only being computed using a single initial state, they are applied to all these simulations because the climatological mean-state biases are not sensitive to internal variability.

e. Analysis methods

Similar to Seager et al. (2022), we use three metrics to measure the tropical Pacific SST change pattern: 1) the zonal gradient index, defined as the SST in a western Pacific box (140° – 170° E, 5° S– 5° N) minus an eastern Pacific box (170° – 90° W, 5° S– 5° N), measuring the zonal west-to-east SST gradient in the equatorial tropical Pacific, so that a positive change in this quantity represents a stronger warming in the western than the eastern Pacific; 2) the meridional gradient index, defined as the difference in the SST between the average off-equatorial boxes for latitudes 10° – 5° S and 5° – 10° N minus an equatorial box for latitude 5° S– 5° N, all for longitudes 170° – 120° W, measuring the equatorial confinement of the lack of warming, or even cooling, in the upwelling region of the central to eastern equatorial

Pacific; 3) the Pacific circulation (PC) index, which is the pattern correlation for the entire equatorial Pacific between 10° S and 10° N, measuring the similarity between observed and modeled trends across the entire equatorial Pacific. The primary period analyzed is 1970–2019 (50 yr) for historical trends, selected to accommodate the start dates of both our experiments and relatively reliable observations. All the results remain consistent when the historical period is set to 1980–2019 or 1980–2022, a focus in many other studies. In this study, trends are computed using linear least squares regression, and their statistical significance is assessed with a two-sided *t* test.

3. Mean-state biases in the tropics

We start by examining how the flux adjustment affects the persistent mean-state biases in CESM2. Figure 1 compares the annual-mean SST, wind stress, and precipitation between observations, CESM2, and CESM2-FA. In common with many other fully coupled climate models, the standard CESM2 exhibits a cold bias in the cold tongue region (Fig. 1c), along with a double ITCZ in precipitation (Fig. 1d) (e.g., Li and Xie 2014). Other prominent (and often shared across other models) biases include the warm bias over the Maritime Continent, cold bias over the northwest Pacific, and the notable warm biases over eastern boundaries of the tropical oceans (Exarchou et al. 2018; Eyring et al. 2021; Zhang et al. 2023). Also note that the pattern of SST biases between the Northern and Southern Hemispheres is more asymmetric in the eastern tropical Pacific than in the western Pacific.

As intended, the flux adjustments applied to CESM2-FA result in significantly smaller SST biases throughout the tropics, particularly there is a reduction of the cold tongue bias, which is the primary concern here (Fig. 1e). The double-ITCZ bias in CESM2 is also largely reduced in CESM2-FA (Fig. 1f), which is associated with the more realistic SSTs and the reduced cross-equatorial northeasterly wind stress (vectors in Figs. 1e,f). Such improvements in simulating the mean state are observed across all 15 members of the CESM2-FA group (not shown), indicating the effectiveness of flux adjustments and the shared mean-state systematic biases across ensemble members. The ensemble-mean tropical Pacific SST and surface wind stress in the two experiments and their difference, which results from the bias reduction through flux adjustments, are further shown in Fig. 2. The mean SST difference between CESM2-FA and CESM2 (Fig. 2c) has the same pattern but with opposite signs compared to the mean SST bias shown in Fig. 1c. That is to say, the different mean state of CESM2-FA results from the reduction of the mean bias in CESM2.

4. The forced responses in the tropical Pacific

In the following, we compare CESM2 and CESM2-FA to examine how the model's mean-state biases can influence the model's forced response in the tropical Pacific. Specifically, we focus on long-term trends in the mean state of the

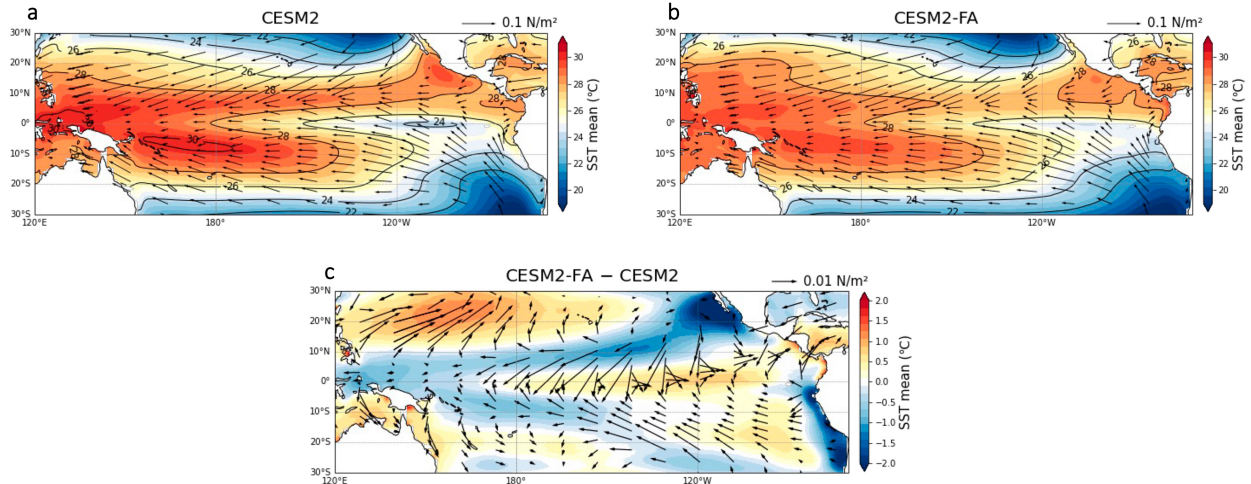


FIG. 2. Annual-mean SST ($^{\circ}\text{C}$) and surface wind stress (N m^{-2}) for (a) CESM2, (b) CESM2-FA, and (c) their difference over 1970–2019.

tropical Pacific climate for both the atmosphere and the ocean.

a. Historical trends in tropical Pacific SST

To contextualize our analysis, we begin with an examination of the discrepancy between observed and modeled Pacific SST trends during the historical period. HadISST observations from 1970 to 2019 indicate a widespread warming

pattern, except for cooling trends in the central to eastern equatorial Pacific and the southeast Pacific, leading to a strengthening tropical Pacific zonal SST gradient (Fig. 3a). In contrast, the modeled forced responses over the same period as derived from the CMIP6 multimodel mean show relatively spatially uniform warming over the tropical Pacific, with opposite (i.e., weakening) trends in the tropical Pacific zonal SST gradient (Fig. 3b). The observed trend toward stronger

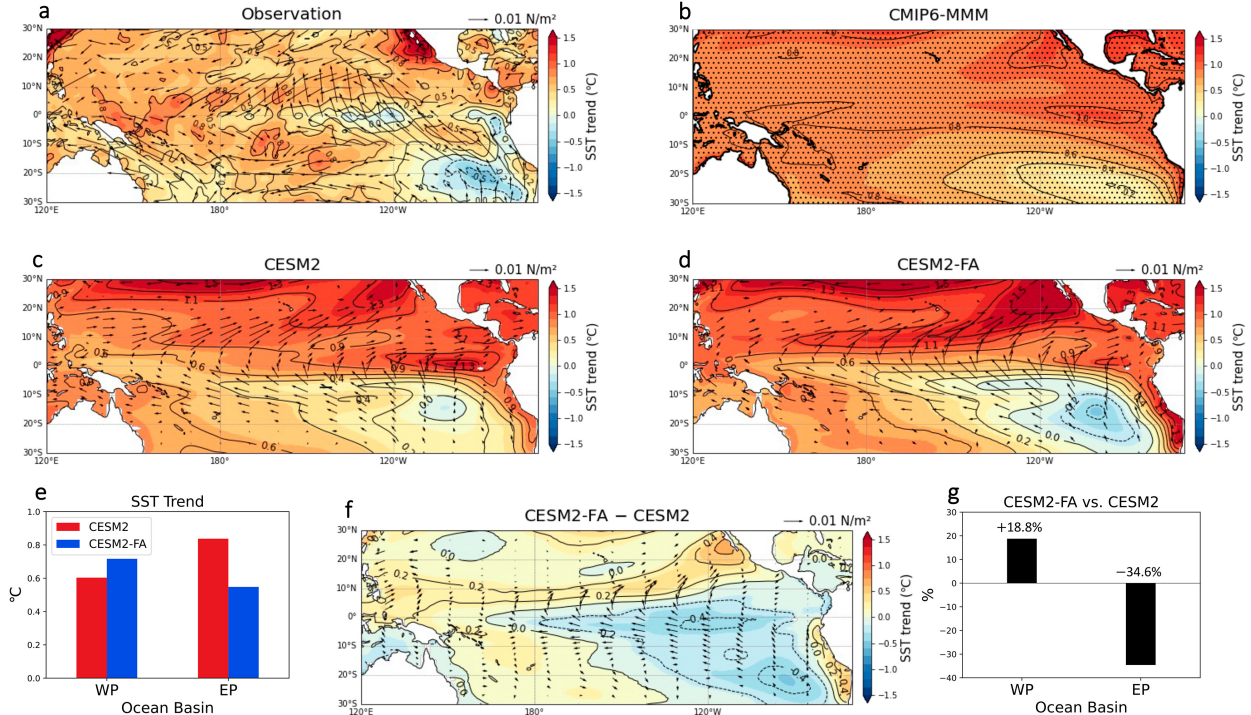


FIG. 3. (a) The tropical Pacific SST trend ($^{\circ}\text{C}$ per 50 years) over 1970–2019 for those from HadISST, (b) multimodel mean trends of CMIP6, (c) CESM2, (d) CESM2-FA, and (f) the difference between the trends of CESM2-FA and CESM2 (CESM2-FA minus CESM2). Shown in (e) is the averaged SST trend over the western Pacific and eastern Pacific (see section 2e for region definition) in CESM2 (red) and CESM2-FA (blue) with their relative difference in (g).

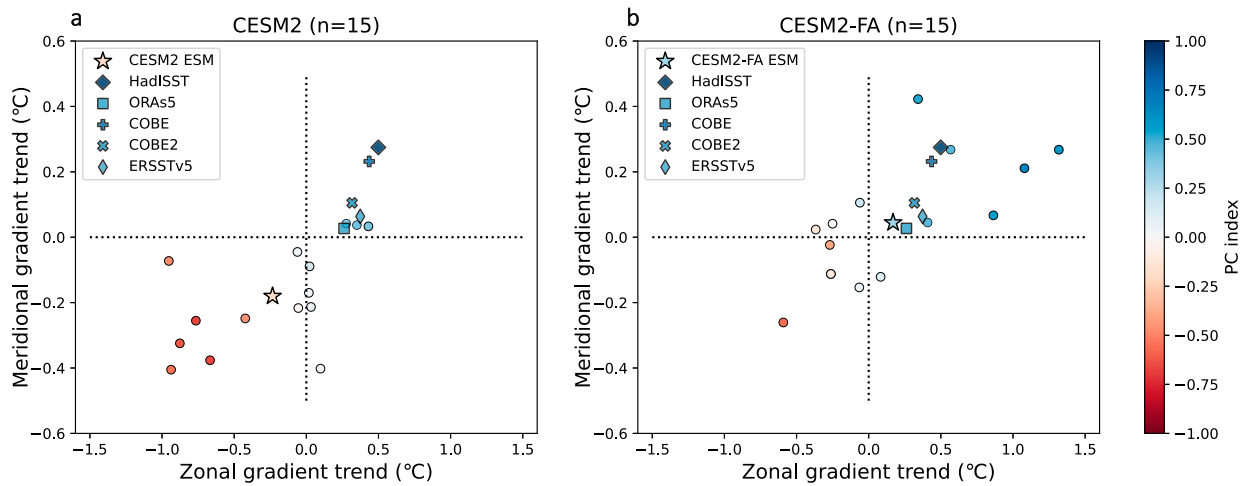


FIG. 4. Scatterplot of trends ($^{\circ}$ C per 50 years) in the equatorial zonal SST gradient (horizontal axis), meridional SST gradient (vertical axis), and the pattern correlation between the HadISST observations-based and modeled SST gradients in the Pacific Ocean 10° S– 10° N domain (color coding of dots), for 1970–2019. Results are shown for (a) CESM2 15 members (dots) and their ensemble mean (ESM; star) and (b) CESM2-FA 15 members (dots) and their ensemble mean (ESM; star). Observation-based estimates from the HadISST, COBE, COBE2, ERSSTv5, and ORAS5 data are also shown in each panel.

zonal SST gradients in the tropical Pacific is often referred to as a La Niña-like pattern, while the trend toward a weaker equatorial Pacific zonal gradient—as projected by most coupled climate models—is called an El Niño-like pattern. Although the physical processes underlying the long-term simulated and observed warming trends differ to some extent from those of seasonal-to-interannual El Niño and La Niña events (e.g., Vecchi and Soden 2007; Lee et al. 2022), we find this terminology useful because it provides clear historical analogs to illustrate the possible teleconnections and impacts, and we continue to use it, while recognizing its limitations.

Over the same period, the 15-member ensemble mean of the standard CESM2 exhibits an El Niño-like SST trend pattern (Fig. 3c), with a 0.84° C warming in the eastern Pacific and 0.60° C warming in the western Pacific (Fig. 3e; red bars). In contrast, the CESM2-FA ensemble mean has a more La Niña-like change (Fig. 3d), with the warming in the western Pacific of 0.72° C exceeding that in the eastern Pacific of 0.55° C (Fig. 3e; blue bars) and so strengthening the zonal SST gradient. The CESM2-FA ensemble mean exhibits a 34.7% decrease in the warming in the eastern Pacific, whereas the western Pacific warming is amplified by 15.7%, both relative to the CESM2 ensemble mean (Fig. 3g). The difference in historical SST trends between CESM2-FA and CESM2 manifests a La Niña-like pattern, characterized by a wedge-shaped cooling extending westward from the eastern Pacific and near the coast of South America (Fig. 3f).

We further examine the tropical Pacific SST trends in each ensemble member of CESM2 and CESM2-FA using the three Pacific SST trend indices defined in section 2e. As shown in Fig. 4, both CESM2 and CESM2-FA present wide ensemble spreads in the tropical Pacific SST trends, reflecting internal variability. In comparison with CESM2, however, the CESM2-FA ensemble members systematically shift toward the upper-right

La Niña-like quadrant, displaying more positive zonal and meridional SST gradient indices, alongside a higher PC index. The difference among the two experiments for all three indices of SST trends passes the 95% significance level. The average trends of the CESM2 ensemble are -0.23 for the zonal gradient, -0.18 for the meridional gradient, and -0.13 for the PC index, while the same metrics are, respectively, 0.17 , 0.05 , and 0.15 for the CESM2-FA. The zonal and meridional gradient trends are 0.50 and 0.27 for HadISST and 0.38 and 0.14 for the observational average. For the zonal tropical Pacific SST gradient trend, specifically, there is only one (6.7%) CESM2 ensemble member that equals or exceeds the averaged observed value, while there are five (33%) such CESM2-FA ensemble members.

Our results provide new evidence that mean-state biases are part of the explanation for the discrepancy in tropical Pacific SST pattern changes between observations and CESM2 (and, by extension, possibly other models). In addition to the enhanced tropical Pacific zonal SST gradient, CESM2-FA exhibits stronger cross-equatorial southeasterly winds and enhanced cooling in the southeastern Pacific (Fig. 3d), which are more consistent with observations (Fig. 3a). Despite applying flux adjustments only to the tropical regions, CESM2-FA also presents reduced Southern Ocean warming (not shown). This suggests that reducing tropical mean-state biases can enhance the model's ability to simulate forced responses that are more consistent with observations in these critical areas. Moreover, these forced response patterns can, in turn, preferentially cool the eastern tropical Pacific and strengthen the zonal SST gradient, for example, through a shortwave cloud feedback (Kang et al. 2023; Kim et al. 2022). Nonetheless, even after mitigating these biases, the CESM2-FA's SST trend (Fig. 3d) does not exactly mirror that in observations (Fig. 3a). This divergence may be attributable to remaining biases in the model, erroneous external (natural and anthropogenic)

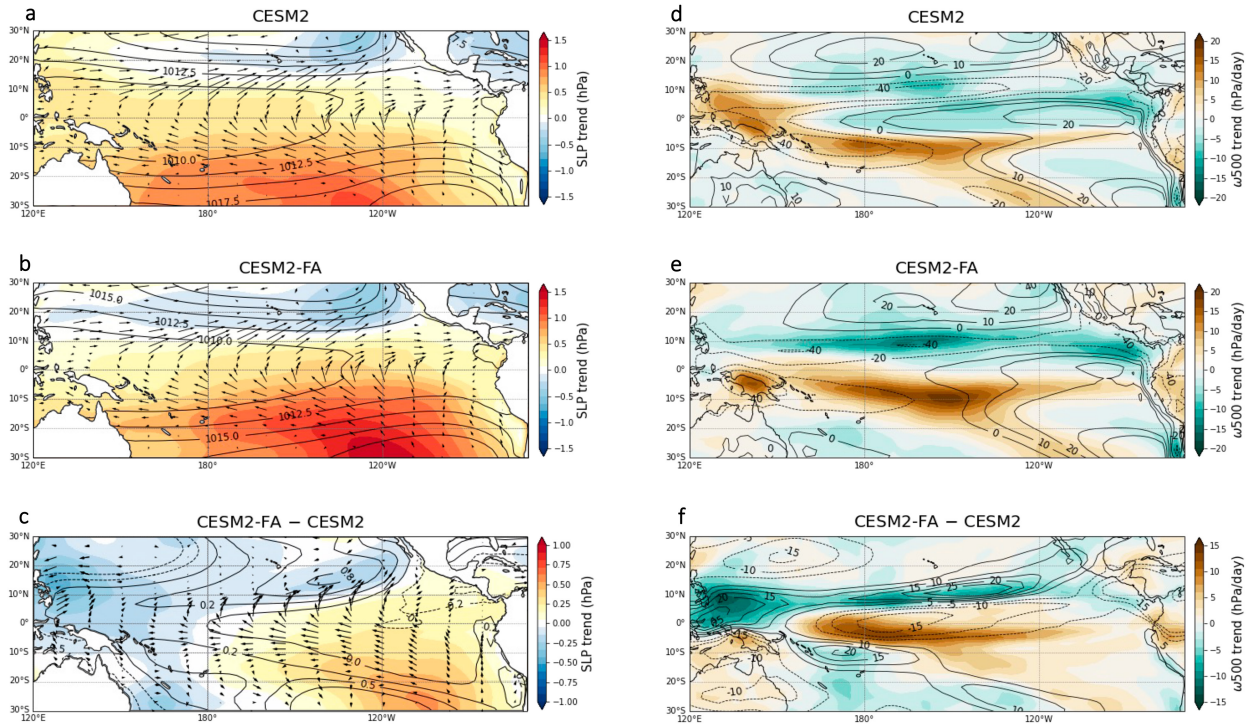


FIG. 5. Trends (shading; per 50 years) and climatology reference (contours) over 1970–2019 for SLP (hPa) in (a) CESM2, (b) CESM2-FA, and (c) their difference (CESM2-FA minus CESM2) and for ω_{500} (hPa day $^{-1}$) in (d) CESM2, (e) CESM2-FA, and (f) their difference (CESM2-FA minus CESM2).

forcings, internal variability (since observations represent only one realization), or a combination of these factors.

b. Historical trends in the Walker circulation and tropical Pacific upper ocean

The tropical Pacific is the site of strong interactions between the ocean and the atmosphere. To better understand how the mean-state biases within CESM2 can contribute to uncertainties in the forced response, we extend our analysis beyond SST to consider the atmospheric Walker circulation and the subsurface upper ocean. For the Walker circulation, we explore trends over 1970–2019 in sea level pressure (SLP), 500-hPa vertical velocity (ω_{500}), and wind stress in CESM2 and CESM2-FA. SLP, which is routinely measured both on land and at sea, along with ω_{500} and wind stress, serve as key indices for evaluating the strength of the Pacific Walker circulation. (e.g., Vecchi and Soden 2007; England et al. 2014). The map of the difference in the SLP trend between CESM2-FA and CESM2 (Fig. 5c) shows an obvious decrease over the western Pacific and an increase over the eastern Pacific, implying an increase in the zonal SLP gradient and an enhancement of the equatorial easterlies. CESM2-FA's tendency toward a more La Niña-like state in the Walker circulation is also evident in the map of ensemble-mean ω_{500} trends (Fig. 5f). Furthermore, the differences in ω_{500} changes (color) between the two experiments are almost everywhere opposite in sign to their respective ω_{500} mean state differences (contour) (Fig. 5f), with a pattern correlation of -0.58 . This

implies that with an overly active convective and ascending background, the Walker circulation in CESM2 slows down more compared to CESM2-FA under identical historical forcing. The mean SST bias—too cold in the eastern Pacific and too warm in the western Pacific—along with the precipitation bias, may also contribute to the model-observation discrepancy in reversed Walker circulation trends. The anticorrelation of the mean state difference and forced response difference in CESM2 and CESM2-FA will be further discussed in section 5.

To provide additional insight on the tropical Pacific climate trends due to the model mean-state biases, we examine ensemble-mean changes in the tropical ocean thermal structure and circulation for CESM2 and CESM2-FA. In both simulations, the GHG-driven warming is trapped near the surface (Figs. 6a,b), suggesting a thermodynamic thermocline shoaling as seen in most climate models (e.g., Vecchi and Soden 2007; Seager et al. 2022). However, significant differences are observed in the tropical oceanic forced responses between the two experiments (Fig. 6c). Among the differences in CESM2-FA relative to CESM2 are 1) enhanced cooling in the upper central to east tropical ocean, 2) enhanced warming of the western equatorial Pacific thermocline and subsurface water, 3) strengthened westward surface currents, 4) increased equatorial upwelling near the central equator, 5) a pronounced enhancement of the east–west thermocline gradient. These characteristics are physically consistent with the intensifying Walker circulation in CESM2-FA as discussed

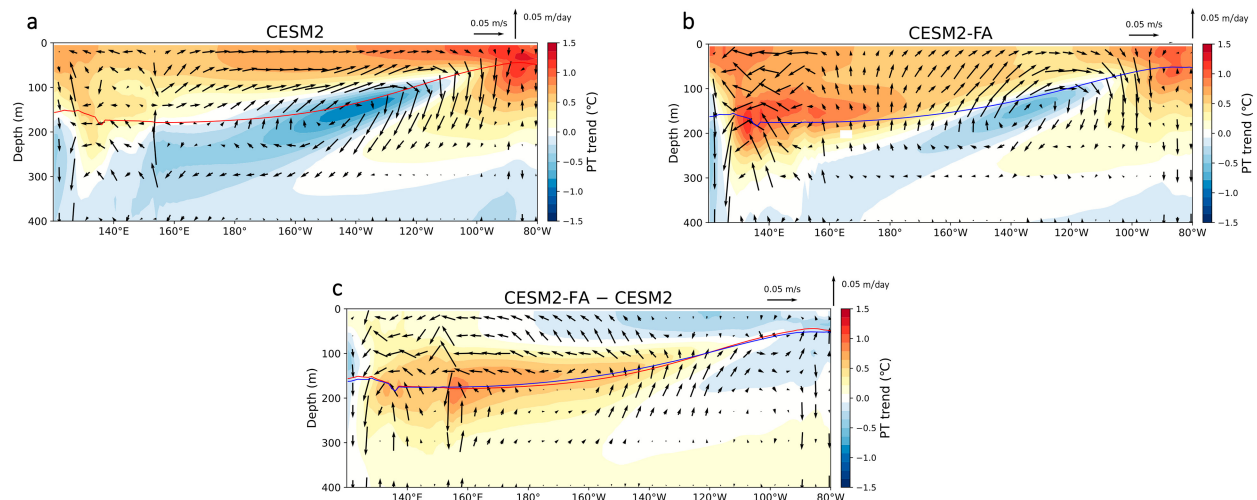


FIG. 6. Trends ($^{\circ}$ C) of equatorial upper-ocean potential temperature over 1971–2019 for (a) CESM2, (b) CESM2-FA, and (c) their difference (CESM2-FA minus CESM2). Red and blue contours indicate 20 $^{\circ}$ C isotherms in the climatological state for CESM2 and CESM2-FA, respectively, measuring the depth of the mean thermocline.

above. The anomalous oceanic trends in the two experiments also reveal an acceleration of the Pacific Ocean shallow overturning cells (not shown) (England et al. 2014), which works to increase both the upwelling of cold waters near the thermocline near the central equatorial region and the subduction of warm water into the western Pacific ventilated thermocline, ultimately increasing subsurface heat uptake in the Pacific while cooling the central to eastern surface layer that interacts with the atmosphere.

Overall, the forced response difference between CESM2 and CESM2-FA is consistent with the ocean thermostat response (Clement et al. 1996; Cane et al. 1997). The enhanced upwelling in CESM2-FA relative to CESM2 (Fig. 6c) advects colder water into the cold tongue, counteracting the warming there and thereby maintaining the strength of the equatorial zonal SST gradient and the Walker circulation. Our findings indicate that the mean-state biases within CESM2 (shared by many coupled climate models) can also contribute to a missing ocean dynamical thermostat cooling effect. When this is missing, the model's response to rising GHGs is toward continuous weakening of the Walker circulation and excessive cold-tongue warming.

5. The anticorrelation between mean state difference and forced response difference

To further examine the relationship between model-observation differences in the mean state and trends, we calculated the pattern correlation between the forced response differences of CESM2 and CESM2-FA and their mean state differences across various physical variables. As shown in Fig. 7, over the historical 50-yr period (1970–2019), all variables exhibit a negative correlation between their ensemble mean trend differences and the mean state differences within the tropical Pacific. Notably, SST displays the most pronounced anticorrelation, with pattern coefficients of -0.68 across the broad 20°N – 20°S belt,

sharpening to -0.81 between 10°N and 10°S , and reaching -0.9 from 5°N to 5°S . This indicates an SST sensitivity that is consistent with the increased thermal damping effect as temperatures rise (Knutson and Manabe 1995), implying that a warmer (colder) mean SST corresponds to slower (faster) warming. This offers an insight of SST sensitivity into how flux adjustments, which reduce the eastern Pacific mean SST cold bias, can possibly reduce eastern Pacific warming and introduce equatorial easterly winds and upwelling anomalies. These conditions could then be further amplified by the Bjerknes feedback, ultimately strengthening the zonal SST gradient. The anticorrelation between ω_{500} mean-state bias and the forced response can also be understood in terms of SST sensitivity. A too-cold cold tongue will have too much subsidence above, while the excessive cold tongue warming induced by the cold tongue bias will lead to anomalous ascent. In addition, there is a significant negative correlation in meridional wind stress (TAUY), indicating that the climatological model bias-modifying trends may also be influenced by the wind–evaporation–SST (WES) feedback (Xie and Philander 1994), particularly given the substantial reduction of the double ITCZ and cross-equatorial northeasterly bias in CESM2-FA.

As summarized in Fig. 8 (left), the mean state difference (CESM2-FA minus CESM2) in SST exhibits an El Niño-like pattern, characterized by a warmer eastern Pacific, reduced easterly winds, a reduced upwelling, thermocline shoaling in the ocean, and a slowing of the Walker circulation. These differences, which have the same pattern but opposite signs to CESM2's mean bias (e.g., Fig. 1b), are induced by flux adjustments. In contrast, the forced response difference between CESM2-FA and CESM2 under identical historical forcing shows a more La Niña-like cooling pattern [Fig. 8 (right)], with a strengthened zonal SST gradient and an enhanced Walker circulation. CESM2-FA also shows enhanced oceanic upwelling, suggesting the unique response pattern is partly

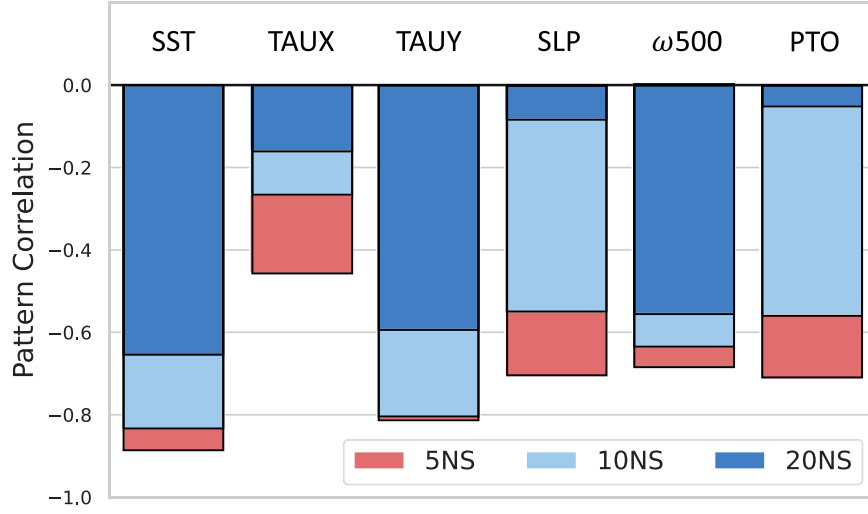


FIG. 7. Pattern correlation between tropical Pacific mean state difference and trend difference between CESM2-FA and CESM2 over 5°S–5°N (red), 10°S–10°N (light blue), and 20°S–20°N (deep blue) for SST, zonal wind stress (TAUX), meridional wind stress (TAUY), SLP, ω_{500} , and potential temperature of ocean (PTO) at tropical equator 0–400-m depth. Both the mean state difference and trend difference are calculated over 1970–2019 using CESM2-FA minus CESM2.

reinforced by the ocean thermostat mechanism (Clement et al. 1996).

Beyond the equatorial region, CESM2-FA exhibits enhanced cooling in the southeastern Pacific and stronger cross-equatorial southeasterly winds [Figs. 3d and 8 (right)], both of which may preferentially cool the central-to-eastern tropical Pacific and further strengthen the tropical Pacific zonal SST gradient. Although flux adjustments were applied only to the tropical regions to reduce mean-state biases, we also expect the extratropics to be influenced through teleconnections

(Alexander 1992; Ding et al. 2011, 2012; Li et al. 2021). Indeed, CESM2-FA also presents reduced Southern Ocean warming compared to CESM2 (not shown), suggesting that two-way teleconnections between the tropical Pacific and Southern Ocean may shape SST patterns in both regions (Kang et al. 2023; Dong et al. 2022). Reduced ITCZ biases may also facilitate the transmission of cooling signals between the equatorial and extraequatorial regions in CESM2-FA.

Overall, our results align well with the main argument of Seager et al. (2019) that the cold tongue warming in state-of-

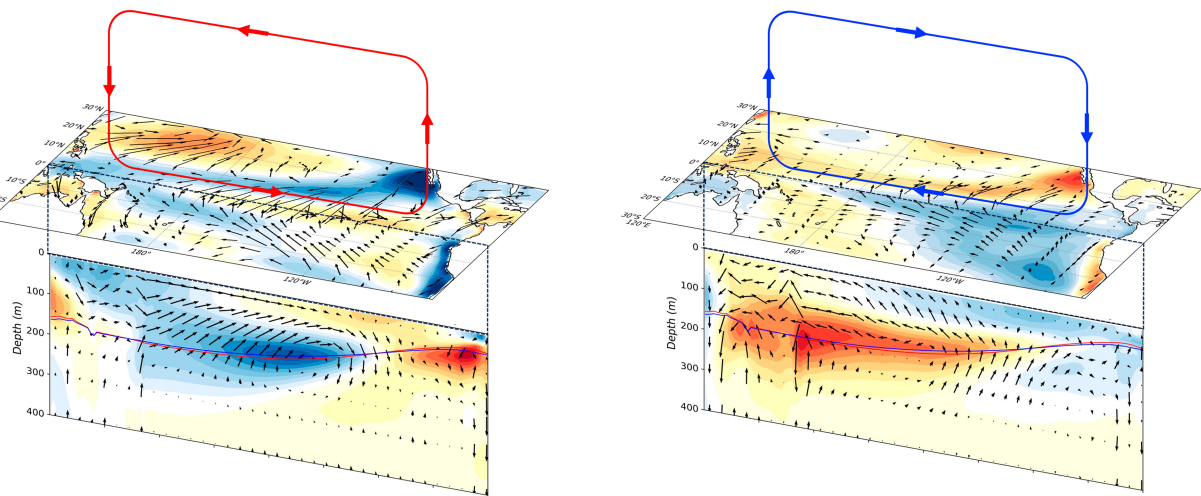


FIG. 8. Schematic overview of the mean state differences (CESM2-FA minus CESM2) in SST and ocean temperature (color), along with (left) wind stress and vertical and horizontal velocity (vectors), and (right) their differences in forced responses over the period 1970–2019. The climatological 20°C thermoclines are shown in red for CESM2 and blue for CESM2-FA. The vertical velocity is magnified for clearer visualization.

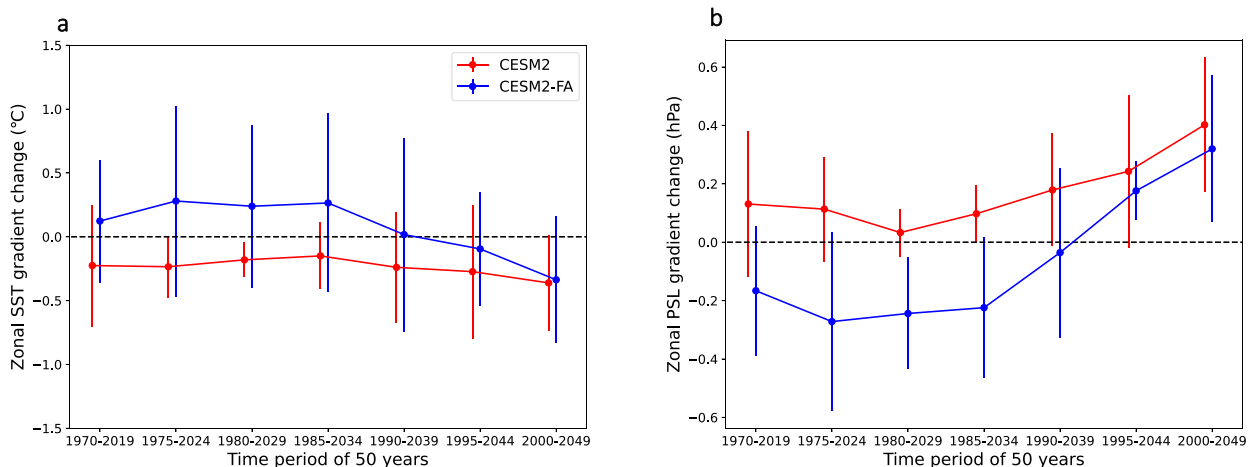


FIG. 9. Linear trends of equatorial zonal (west-east) gradient in (a) SST and (b) SLP for 50 years with a sliding window between 1970 and 2049 in CESM2 (red) and CESM2-FA (blue). Ensemble-mean values of the trends are represented by dots and solid curves, with error bars indicating 2 times of the standard deviation of the 15 member ensemble spread.

the-art models is due to the too-cold cold tongue bias. However, the mechanisms by which mean-state biases influence the historical forced response in CESM2 appear more complex than those proposed in Seager et al. (2019) and warrant further research. It is worth noting that, despite the background differences between CESM2-FA and CESM2 [Figs. 2c and 8 (left)]—induced by flux adjustments and related to mean biases—remain consistent across different periods, the forced response can evolve, as will be shown in the next section.

6. Transience of the La Niña-like change

Theories and previous studies based on model simulations have suggested that the role of the oceanic thermostat can be temporary. The upwelling water in the cold tongue originates primarily from the subtropical gyre region, where it subducts from the ocean mixed layer before flowing toward the equator in the subsurface layers of the shallow subtropical cells (McCreary and Lu 1994; Rodgers et al. 2003). This route can take decades (e.g., Thomas and Fedorov 2017). Therefore, the warming of the upwelling waters lags that of the SST in the subtropical subduction region by decades, but once the extratropical oceans have adjusted to the warming, the stronger zonal SST gradient can no longer persist in competition with other mechanisms that seek to weaken the zonal SST gradient (Heede et al. 2020, 2021). Other processes, such as the aerosol forcing (e.g., Heede and Fedorov 2021; Hwang et al. 2024) and the Southern Ocean cooling (e.g., Bronselaer et al. 2018), may also lead to a shift in the tropical Pacific SST change pattern. Here, we explore this hypothesis using the 80 years (1970–2049) simulations of CESM2 and CESM2-FA with 15 ensemble members. Linear trends of the equatorial west–east SST gradient (see section 2e for definition) calculated over 50-yr moving windows shift from positive to negative approximately around 2040 in CESM2-FA (Fig. 9a), indicating that the La Niña-like tendency with strengthening tropical Pacific zonal SST gradient in CESM2-FA has a

transient nature. In contrast, CESM2's ensemble-mean zonal SST gradient trends remain consistently negative throughout the full period. The difference in trends is relatively consistent up to 2035 but diminishes thereafter. A consistent result was obtained for the zonal gradient trends of SLP using the same west–east domain boxes (Fig. 9b). This result suggests a tendency for CESM2-FA to have an enhanced Walker circulation over the tropical Pacific up to approximately around 2040. However, this result does not indicate that the observed La Niña-like trends will end in the near-term future, since the observed subsurface cooling with cold upwelling waters in the equatorial Pacific (Seager et al. 2022; Jiang et al. 2024) is stronger and colder than that detected in the CESM2-FA simulations (Fig. 6b). In addition, we also observe that the internal variance increases in CESM2-FA (error bars in Fig. 6), which is associated with a better simulation of the dominant ENSO periodicity that aligns more closely with observations (not shown). In contrast, the ENSO periodicity in CESM2 tends to be too short. But both CESM2 and CESM2-FA simulate much larger ENSO amplitude (in terms of the standard deviation of Niño-3.4 SSTA) than observations.

7. Conclusions

In this study, we identify different radiatively forced trends in the tropical Pacific in a fully coupled climate model and its flux-corrected counterpart. The fully coupled model has a trend toward a reduced zonal SST gradient in the equator. In contrast, in the bias-corrected model, there is a more La Niña-like strengthening of the Pacific zonal SST gradient, coupled with an enhanced Walker circulation and an ocean thermostat-like response, thus shifting the modeled trends closer to observations. We examine the tropical Pacific states across two sets of ensemble experiments and note that a specific pattern of background bias is responsible for skewing the forced response trend pattern. Namely, the La Niña-like mean-state bias—characterized by an excessively cold tongue

and an overly warm warm pool—may predispose this climate model, and by extension perhaps others—to an El Niño-like forced response. Ocean–atmosphere interactions, including the Bjerknes feedback, may amplify the models’ initial historical forcing response leading to opposite signed changes in the zonal SST gradient and Walker circulation in the two model versions. Overall, our findings support the main argument by Seager et al. (2019) that common mean-state biases in climate models influence the simulated response of the climate system to radiative forcing. However, the mechanisms by which mean-state biases affect the historical forced response in CESM2 have not been fully analyzed here and may be more complex than those proposed by Seager et al. (2019), given the use of a coupled Earth system model with evolving historical forcings—in contrast to the simplified atmosphere–ocean coupled model driven by increasing CO₂ as used in Seager et al. (2019). Further research will examine the processes through which CESM2-FA produces a more La Niña-like historical trend.

Our findings are based on a single model (CESM2), and the characteristics of the mean-state bias and trend bias identified here remain to be tested and compared with other models and different forcing schemes. Possible contributions from teleconnections between the tropical Pacific and broader global regions (e.g., Dong et al. 2022; Kang et al. 2023), as well as the attribution of individual forcing (e.g., Deser et al. 2020; Heede and Fedorov 2021; Hwang et al. 2024), are not addressed here but will be explored in our future work. Despite these caveats, our work based on ensemble simulations raises the possibility that the recent trend toward more La Niña-like conditions may partially be driven by forced climate change. In addition, we need to conduct further analysis to explain the different climate sensitivities resulting from the bias-induced background diversity in CESM2 and CESM2-FA.

The simulations based on CESM2-FA also indicate that the strengthening of zonal SST and SLP gradients in response to radiative forcing is transient. However, it remains uncertain whether the model can realistically simulate the delayed warming of subsurface temperatures. For adaptation and mitigation purposes, transient adjustments of the climate system are of greater importance than its equilibrium responses. Consequently, it is crucial to advance the development of climate models to reduce systematic biases that could lead to errors in the forced Pacific trends. For example, gains in better simulation of the tropical Pacific perhaps will come from moving

toward higher spatial resolution (Wengel et al. 2021; Yeager et al. 2023) as computers get cheaper and faster. Although there are no simple solutions to this challenge, we stress the importance of accounting for the uncertainties associated with the tropical Pacific’s forced response when applying climate projections for climate risk adaptation. In addition, our results suggest that flux adjustment may be an effective method to develop alternative projections that represent a broader range of possible future tropical Pacific warming scenarios. These projections will also be valuable for understanding regional patterns of climate risk in the short to medium term, including the potential impacts of tropical cyclones and other extreme weather events (Sobel et al. 2023).

Acknowledgments. The authors would like to acknowledge the support of the NSF (AGS-2217618 and AGS-2217620) and the U.S. Department of Energy (DOE) (DE-SC0023333). We acknowledge high-performance computing support from the Derecho system (<https://doi.org/10.5065/qx9a-pg09>) provided by the NSF National Center for Atmospheric Research (NCAR), sponsored by the National Science Foundation. This research also used resources of the National Energy Research Scientific Computing Center (NERSC), a DOE Office of Science User Facility using NERSC Award BER-ERCAP0032323.

Data availability statement. 1) CMIP6 data were retrieved from the Earth System Grid Federation (<https://esgf-node.llnl.gov/projects/cmip6/>). 2) The CESM2 restart files used for generating our simulations can be found at https://svn-ccsm-inputdata.cgd.ucar.edu/trunk/inputdata/cesm2_init/. 3) All codes used for data analysis and figures are available online (<https://github.com/jingyizhuo>). 4) Monthly outputs from the flux adjustment experiments are available from J.-Y. Z. on request.

APPENDIX

The Climatological Flux Adjustments Imposed to Build CESM2-FA

Figure A1 shows the annual mean and seasonal cycle of the heat and momentum flux adjustments applied to build CESM2-FA.

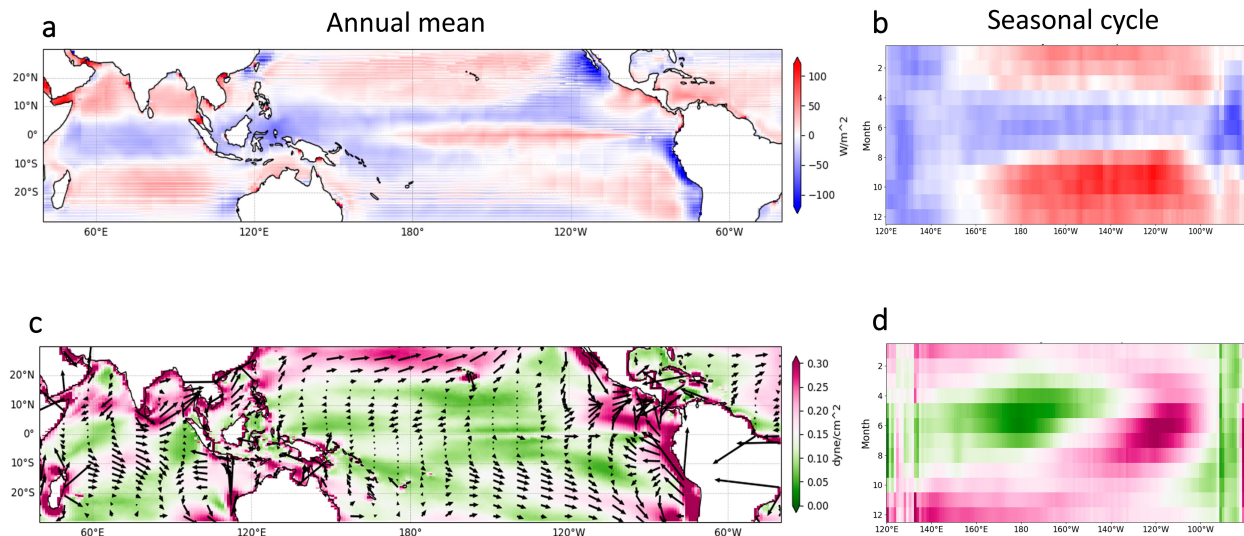


FIG. A1. (a), (b) The climatological heat flux (W m^{-2}) and (c), (d) wind stress (dyne cm^{-2} ; vectors show direction and shading shows magnitude) adjustments imposed to build CESM2-FA. (left) The annual mean of flux adjustments over the whole tropics. (right) The seasonal cycle on the tropical equator (5°S – 5°N).

REFERENCES

- Alexander, M. A., 1992: Midlatitude atmosphere–ocean interaction during El Niño. Part I: The North Pacific Ocean. *J. Climate*, **5**, 944–958, [https://doi.org/10.1175/1520-0442\(1992\)005<0944:MAIDEN>2.0.CO;2](https://doi.org/10.1175/1520-0442(1992)005<0944:MAIDEN>2.0.CO;2).
- Betts, A. K., 1998: Climate-convection feedbacks: Some further issues. *Climatic Change*, **39**, 35–38, <https://doi.org/10.1023/A:1005323805826>.
- Bjerknes, J., 1966: A possible response of the atmospheric Hadley circulation to equatorial anomalies of ocean temperature. *Tellus*, **18A**, 820–829, <https://doi.org/10.3402/tellusa.v18i4.9712>.
- Bordbar, M. H., T. Martin, M. Latif, and W. Park, 2017: Role of internal variability in recent decadal to multidecadal tropical Pacific climate changes. *Geophys. Res. Lett.*, **44**, 4246–4255, <https://doi.org/10.1002/2016GL072355>.
- Bronselaeer, B., M. Winton, S. M. Griffies, W. J. Hurlin, K. B. Rodgers, O. V. Sergienko, R. J. Stouffer, and J. L. Russell, 2018: Change in future climate due to Antarctic meltwater. *Nature*, **564**, 53–58, <https://doi.org/10.1038/s41586-018-0712-z>.
- Cane, M. A., A. C. Clement, A. Kaplan, Y. Kushnir, D. Pozdnyakov, R. Seager, S. E. Zebiak, and R. Murtugudde, 1997: Twentieth-century sea surface temperature trends. *Science*, **275**, 957–960, <https://doi.org/10.1126/science.275.5302.957>.
- Clement, A. C., R. Seager, M. A. Cane, and S. E. Zebiak, 1996: An ocean dynamical thermostat. *J. Climate*, **9**, 2190–2196, [https://doi.org/10.1175/1520-0442\(1996\)009<2190:AODT>2.0.CO;2](https://doi.org/10.1175/1520-0442(1996)009<2190:AODT>2.0.CO;2).
- Danabasoglu, G., and Coauthors, 2020: The Community Earth System Model Version 2 (CESM2). *J. Adv. Model. Earth Syst.*, **12**, e2019MS001916, <https://doi.org/10.1029/2019MS001916>.
- Deser, C., and Coauthors, 2020: Isolating the evolving contributions of anthropogenic aerosols and greenhouse gases: A new CESM1 large ensemble community resource. *J. Climate*, **33**, 7835–7858, <https://doi.org/10.1175/JCLI-D-20-0123.1>.
- Ding, Q., E. J. Steig, D. S. Battisti, and M. Küttel, 2011: Winter warming in West Antarctica caused by central tropical Pacific warming. *Nat. Geosci.*, **4**, 398–403, <https://doi.org/10.1038/ngeo1129>.
- , —, —, and J. M. Wallace, 2012: Influence of the tropics on the southern annular mode. *J. Climate*, **25**, 6330–6348, <https://doi.org/10.1175/JCLI-D-11-00523.1>.
- Dong, Y., K. C. Armour, D. S. Battisti, and E. Blanchard-Wrigglesworth, 2022: Two-way teleconnections between the Southern Ocean and the tropical Pacific via a dynamic feedback. *J. Climate*, **35**, 6267–6282, <https://doi.org/10.1175/JCLI-D-22-0080.1>.
- England, M. H., and Coauthors, 2014: Recent intensification of wind-driven circulation in the Pacific and the ongoing warming hiatus. *Nat. Climate Change*, **4**, 222–227, <https://doi.org/10.1038/nclimate2106>.
- Exarchou, E., C. Prodhomme, L. Brodeau, V. Guemas, and F. Doblas-Reyes, 2018: Origin of the warm eastern Tropical Atlantic SST bias in a climate model. *Climate Dyn.*, **51**, 1819–1840, <https://doi.org/10.1007/s00382-017-3984-3>.
- Eyring, V., S. Bony, G. A. Meehl, C. A. Senior, B. Stevens, R. J. Stouffer, and K. E. Taylor, 2016: Overview of the Coupled Model Intercomparison Project Phase 6 (CMIP6) experimental design and organization. *Geosci. Model Dev.*, **9**, 1937–1958, <https://doi.org/10.5194/gmd-9-1937-2016>.
- , —, and Coauthors, 2021: Human influence on the climate system. *Climate Change 2021: The Physical Science Basis*, V. Masson-Delmotte et al., Eds., Cambridge University Press, 423–552, <https://doi.org/10.1017/9781009157896>.
- Heede, U. K., and A. V. Fedorov, 2021: Eastern equatorial Pacific warming delayed by aerosols and thermostat response to CO₂ increase. *Nat. Climate Change*, **11**, 696–703, <https://doi.org/10.1038/s41558-021-01101-x>.
- , —, and N. J. Burls, 2020: Time scales and mechanisms for the tropical Pacific response to global warming: A tug of war between the ocean thermostat and weaker Walker. *J. Climate*, **33**, 6101–6118, <https://doi.org/10.1175/JCLI-D-19-0690.1>.
- , —, and —, 2021: A stronger versus weaker Walker: Understanding model differences in fast and slow tropical

- Pacific responses to global warming. *Climate Dyn.*, **57**, 2505–2522, <https://doi.org/10.1007/s00382-021-05818-5>.
- Hersbach, H., and Coauthors, 2020: The ERA5 global reanalysis. *Quart. J. Roy. Meteor. Soc.*, **146**, 1999–2049, <https://doi.org/10.1002/qj.3803>.
- Hirahara, S., M. Ishii, and Y. Fukuda, 2014: Centennial-scale sea surface temperature analysis and its uncertainty. *J. Climate*, **27**, 57–75, <https://doi.org/10.1175/JCLI-D-12-00837.1>.
- Hu, S., and A. V. Fedorov, 2017: The extreme El Niño of 2015–2016 and the end of global warming hiatus. *Geophys. Res. Lett.*, **44**, 3816–3824, <https://doi.org/10.1002/2017GL072908>.
- Huang, B., and Coauthors, 2015: Extended Reconstructed Sea Surface Temperature version 4 (ERSST.V4). Part I: Upgrades and intercomparisons. *J. Climate*, **28**, 911–930, <https://doi.org/10.1175/JCLI-D-14-00006.1>.
- Hwang, Y.-T., S.-P. Xie, P.-J. Chen, H.-Y. Tseng, and C. Deser, 2024: Contribution of anthropogenic aerosols to persistent La Niña-like conditions in the early 21st century. *Proc. Natl. Acad. Sci. USA*, **121**, e2315124121, <https://doi.org/10.1073/pnas.2315124121>.
- Ishii, M., A. Shouji, S. Sugimoto, and T. Matsumoto, 2005: Objective analyses of sea-surface temperature and marine meteorological variables for the 20th century using ICOADS and the Kobe Collection. *Int. J. Climatol.*, **25**, 865–879, <https://doi.org/10.1002/joc.1169>.
- Jiang, F., R. Seager, and M. A. Cane, 2024: Historical subsurface cooling in the tropical Pacific and its dynamics. *J. Climate*, **37**, 5925–5938, <https://doi.org/10.1175/JCLI-D-24-0007.1>.
- Kang, S. M., S.-P. Xie, Y. Shin, H. Kim, Y.-T. Hwang, M. F. Stuecker, B. Xiang, and M. Hawcroft, 2020: Walker circulation response to extratropical radiative forcing. *Sci. Adv.*, **6**, eabd3021, <https://doi.org/10.1126/sciadv.abd3021>.
- , Y. Yu, C. Deser, X. Zhang, I.-S. Kang, S.-S. Lee, K. B. Rodgers, and P. Ceppi, 2023: Global impacts of recent Southern Ocean cooling. *Proc. Natl. Acad. Sci. USA*, **120**, e2300881120, <https://doi.org/10.1073/pnas.2300881120>.
- Kay, J. E., and Coauthors, 2015: The Community Earth System Model (CESM) large ensemble project: A community resource for studying climate change in the presence of internal climate variability. *Bull. Amer. Meteor. Soc.*, **96**, 1333–1349, <https://doi.org/10.1175/BAMS-D-13-00255.1>.
- Kim, H., S. M. Kang, J. E. Kay, and S.-P. Xie, 2022: Subtropical clouds key to Southern Ocean teleconnections to the tropical Pacific. *Proc. Natl. Acad. Sci. USA*, **119**, e2200514119, <https://doi.org/10.1073/pnas.2200514119>.
- Knutson, T. R., and S. Manabe, 1995: Time-mean response over the tropical Pacific to increased CO₂ in a coupled ocean-atmosphere model. *J. Climate*, **8**, 2181–2199, [https://doi.org/10.1175/1520-0442\(1995\)008<2181:TMROTT>2.0.CO;2](https://doi.org/10.1175/1520-0442(1995)008<2181:TMROTT>2.0.CO;2).
- Kosaka, Y., and S.-P. Xie, 2013: Recent global-warming hiatus tied to equatorial Pacific surface cooling. *Nature*, **501**, 403–407, <https://doi.org/10.1038/nature12534>.
- Lee, S., M. L'Heureux, A. T. Wittenberg, R. Seager, P. A. O'Gorman, and N. C. Johnson, 2022: On the future zonal contrasts of equatorial Pacific climate: Perspectives from observations, simulations, and theories. *npj Climate Atmos. Sci.*, **5**, 82, <https://doi.org/10.1038/s41612-022-00301-2>.
- Li, G., and S.-P. Xie, 2014: Tropical biases in CMIP5 multimodel ensemble: The excessive equatorial Pacific cold tongue and double ITCZ problems. *J. Climate*, **27**, 1765–1780, <https://doi.org/10.1175/JCLI-D-13-00337.1>.
- Li, X., and Coauthors, 2021: Tropical teleconnection impacts on Antarctic climate changes. *Nat. Rev. Earth Environ.*, **2**, 680–698, <https://doi.org/10.1038/s43017-021-00204-5>.
- Magnusson, L., M. Alonso-Balmaseda, S. Corti, F. Molteni, and T. Stockdale, 2013: Evaluation of forecast strategies for seasonal and decadal forecasts in presence of systematic model errors. *Climate Dyn.*, **41**, 2393–2409, <https://doi.org/10.1007/s00382-012-1599-2>.
- McCreary, J. P., Jr., and P. Lu, 1994: Interaction between the subtropical and equatorial ocean circulations: The subtropical cell. *J. Phys. Oceanogr.*, **24**, 466–497, [https://doi.org/10.1175/1520-0485\(1994\)024<0466:IBTSAE>2.0.CO;2](https://doi.org/10.1175/1520-0485(1994)024<0466:IBTSAE>2.0.CO;2).
- Murakami, H., T. L. Delworth, W. F. Cooke, M. Zhao, B. Xiang, and P.-C. Hsu, 2020: Detected climatic change in global distribution of tropical cyclones. *Proc. Natl. Acad. Sci. USA*, **117**, 10 706–10 714, <https://doi.org/10.1073/pnas.1922500117>.
- Olonscheck, D., M. Rugenstein, and J. Marotzke, 2020: Broad consistency between observed and simulated trends in sea surface temperature patterns. *Geophys. Res. Lett.*, **47**, e2019GL086773, <https://doi.org/10.1029/2019GL086773>.
- Rayner, N. A., D. E. Parker, E. B. Horton, C. K. Folland, L. V. Alexander, D. P. Rowell, E. C. Kent, and A. Kaplan, 2003: Global analyses of sea surface temperature, sea ice, and night marine air temperature since the late nineteenth century. *J. Geophys. Res.*, **108**, 4407, <https://doi.org/10.1029/2002JD002670>.
- Rodgers, K. B., B. Blanke, G. Madec, O. Aumont, P. Caias, and J.-C. Dutay, 2003: Extratropical sources of equatorial Pacific upwelling in an OGCM. *Geophys. Res. Lett.*, **30**, 1084, <https://doi.org/10.1029/2002GL016003>.
- , and Coauthors, 2021: Ubiquity of human-induced changes in climate variability. *Earth Syst. Dyn.*, **12**, 1393–1411, <https://doi.org/10.5194/esd-12-1393-2021>.
- Sarachik, E. S., and M. A. Cane, 2010: *The El Niño–Southern Oscillation Phenomenon*. Cambridge University Press, 369 pp.
- Schneider, D. P., C. Deser, J. Fasullo, and K. E. Trenberth, 2013: Climate data guide spurs discovery and understanding. *Eos, Trans. Amer. Geophys. Union*, **94**, 121–122, <https://doi.org/10.1029/2013EO130001>.
- Seager, R., M. Cane, N. Henderson, D.-E. Lee, R. Abernathey, and H. Zhang, 2019: Strengthening tropical Pacific zonal sea surface temperature gradient consistent with rising greenhouse gases. *Nat. Climate Change*, **9**, 517–522, <https://doi.org/10.1038/s41558-019-0505-x>.
- , N. Henderson, and M. Cane, 2022: Persistent discrepancies between observed and modeled trends in the tropical Pacific Ocean. *J. Climate*, **35**, 4571–4584, <https://doi.org/10.1175/JCLI-D-21-0648.1>.
- , M. Ting, P. Alexander, H. Liu, J. Nakamura, C. Li, and M. Newman, 2023: Ocean-forcing of cool season precipitation drives ongoing and future decadal drought in southwestern North America. *npj Climate Atmos. Sci.*, **6**, 141, <https://doi.org/10.1038/s41612-023-00461-9>.
- Sobel, A. H., and Coauthors, 2023: Near-term tropical cyclone risk and coupled Earth system model biases. *Proc. Natl. Acad. Sci. USA*, **120**, e2209631120, <https://doi.org/10.1073/pnas.2209631120>.
- Spencer, H., R. Sutton, and J. M. Slingo, 2007: El Niño in a coupled climate model: Sensitivity to changes in mean state induced by heat flux and wind stress corrections. *J. Climate*, **20**, 2273–2298, <https://doi.org/10.1175/JCLI4111.1>.
- Thomas, M. D., and A. V. Fedorov, 2017: The eastern subtropical Pacific origin of the equatorial cold bias in climate models: A

- Lagrangian perspective. *J. Climate*, **30**, 5885–5900, <https://doi.org/10.1175/JCLI-D-16-0819.1>.
- Vecchi, G. A., and B. J. Soden, 2007: Global warming and the weakening of the tropical circulation. *J. Climate*, **20**, 4316–4340, <https://doi.org/10.1175/JCLI4258.1>.
- , and Coauthors, 2014: On the seasonal forecasting of regional tropical cyclone activity. *J. Climate*, **27**, 7994–8016, <https://doi.org/10.1175/JCLI-D-14-00158.1>.
- Watanabe, M., J.-L. Dufresne, Y. Kosaka, T. Mauritsen, and H. Tatebe, 2021: Enhanced warming constrained by past trends in equatorial Pacific sea surface temperature gradient. *Nat. Climate Change*, **11**, 33–37, <https://doi.org/10.1038/s41558-020-00933-3>.
- Wengel, C., S.-S. Lee, M. F. Stuecker, A. Timmermann, J.-E. Chu, and F. Schloesser, 2021: Future high-resolution El Niño–Southern Oscillation dynamics. *Nat. Climate Change*, **11**, 758–765, <https://doi.org/10.1038/s41558-021-01132-4>.
- Wills, R. C. J., Y. Dong, C. Proistosecu, K. C. Armour, and D. S. Battisti, 2022: Systematic climate model biases in the large-scale patterns of recent sea-surface temperature and sea-level pressure change. *Geophys. Res. Lett.*, **49**, e2022GL100011, <https://doi.org/10.1029/2022GL100011>.
- Xie, S.-P., and S. G. H. Philander, 1994: A coupled ocean-atmosphere model of relevance to the ITCZ in the eastern Pacific. *Tellus*, **46A**, 340–350, <https://doi.org/10.3402/tellusa.v46i4.15484>.
- , C. Deser, G. A. Vecchi, J. Ma, H. Teng, and A. T. Wittenberg, 2010: Global warming pattern formation: Sea surface temperature and rainfall. *J. Climate*, **23**, 966–986, <https://doi.org/10.1175/2009JCLI329.1>.
- Yeager, S. G., and Coauthors, 2023: Reduced Southern Ocean warming enhances global skill and signal-to-noise in an eddy-resolving decadal prediction system. *npj Climate Atmos. Sci.*, **6**, 107, <https://doi.org/10.1038/s41612-023-00434-y>.
- Zhang, Q., B. Liu, S. Li, and T. Zhou, 2023: Understanding models' global sea surface temperature bias in mean state: From CMIP5 to CMIP6. *Geophys. Res. Lett.*, **50**, e2022GL100888, <https://doi.org/10.1029/2022GL100888>.